Rough Set Based Approach for IMT Automatic Estimation

Samanta Rosati[a], Filippo Molinari[a], Gabriella Balestra[a]

[a]Departement of Electronics and Telecommunications, Politecnico di Torino, Torino, Italy

Correspondence: S Rosati, Department of Electronics and Telecommunications, Politecnico di Torino, corso Duca degli Abruzzi 24, 10129 Torino, Italy. E-mail: samanta.rosati@polito.it, phone +39 011 090 4207

Abstract. Carotid artery (CA) intima-media thickness (IMT) is commonly deemed as one of the risk marker for cardiovascular diseases. The automatic estimation of the IMT on ultrasound images is based on the correct identification of the lumen-intima (LI) and media-adventitia (MA) interfaces. This task is complicated by noise, vessel morphology and pathology of the carotid artery.

In a previous study we applied four non-linear methods for feature selection on a set of variables extracted from ultrasound carotid images. The main aim was to select those parameters containing the highest amount of information useful to classify the image pixels in the carotid regions they belong to.

In this study we present a pixel classifier based on the selected features. Once the pixels classification was correctly performed, the IMT was evaluated and compared with two sets of manual-traced profiles. The results showed that the automatic IMTs are not statistically different from the manual ones.

Keywords: Classification; Feature Selection; Image Segmentation; QuickReduct Algorithm; Rough Set Theory

1. Introduction

The intima-media thickness (IMT) of the carotid artery (CA) is the most widely used indicator for cardiovascular diseases [Touboul et al., 2004]. Therefore, an accurate segmentation of the CA wall performed on ultrasound images results an important step in measuring the IMT of patients.

Tools for the automated and completely user-independent segmentation techniques are gaining increasing importance because they avoid the bias coming from human interactions. However, automated techniques still underperform with respect to semi-automated IMT measurement methods because of the images variability introduced by noise, vessel morphology and pathology. Hence, it could be useful to encapsulate in these algorithms some kind of intelligence in order to overcome the mentioned problems and improve the final performances.

Feature selection is a procedure allowing to highlight the relevant parameters in multivariate data, containing knowledge useful for the classification process. All other variables result irrelevant for the final purpose or redundant, that is highly correlated with other features and interchangeable with them. Moreover they could be sources of noise for the following analysis phases performed on data, masking those aspects really important in data.

In [Rosati et al., 2011] we performed feature selection on carotid ultrasound images in order to extract the most informative parameters for the pixels classification in one of the three carotid layers of interest: lumen, intima-media complex and adventitia.

In this study we use the selected set of features to automatically segment ultrasound images. Firstly, a classifier based on Artificial Neural Networks (ANNs) was built, able to identify the carotid region each pixel belongs to. Afterwards, the lumen-intima (LI) and media-adventitia (MA) interfaces were automatically traced based on the pixels classification and the IMT was calculated.

2. Methods

We tested a data base consisting of 300 images coming from different institutions. One hundred images were acquired at the Neurology Division of Nicosia (Cyprus) from 100 healthy subjects (age:

54±24, 60 males) and 200 from the Neurology Dept. of the Gradenigo Hospital of Torino (Italy) from 150 patients (age: 69±16, 97 males). All the images were discretized on 8 bits (grayscale from 0 to 255) and digitally sent to a computer. The conversion factor for Nicosia images was 0.06 mm/pixel, that of Torino was 0.0625 mm/pixel. Our database comprised both normal carotids (i.e., with an IMT lower than 0.85 mm and no plaques) as well as pathologic vessels. Our database comprised both normal carotids (i.e., with an IMT lower than 0.85 mm and no plaques) and pathologic vessels. Also, all carotid morphologies were included: straight and horizontal, curved, and inclined arteries. Finally, we had images with a good signal-to-noise ratio and also images with a high degree of blood backscattering.

2.1. Feature Extraction and Selection

In this study we identified four different classes of pixels, according to their physiological meaning: lumen, intima-media complex, adventitia and noisy lumen. The last class of pixels was included in order to properly manage also those images with a low signal-to-noise ratio.

In order to build a dataset on which to perform feature selection, 600 pixels per class were randomly chosen from 60 images randomly selected. For each single pixel, other than its intensity, we considered as features different parameters essentially based on the intensity of the pixels around it and belonging to two categories: statistical moments estimates and texture features. Texture gives important information that humans use in analyzing a scene [Amadasun and King, 1989]. Particularly, texture features are a set of digital parameters based on the spatial displacement of the intensity levels in an image. They are based on the Grey Level Co-occurrence Matrix (GLCM) [Tan et al., 2010].

A list of the image descriptors used in this work is given below:
1. Intensity of the single pixel.
2. Statistical moments: mean value, standard deviation, skewness, and kurtosis.
3. Spatial Gray Level Dependence Method (SGLDM) [Conners and Harlow, 1980] with a displacement $\delta=(0,1)$: energy, contrast, homogeneity, entropy, and first, third and fourth order moments.
4. Gray Level Difference Method (GLDM) [Conners and Harlow, 1980] with a displacement $\delta=(0,1)$: contrast, angular second moment, entropy, and mean.
5. Gray Level Run Length Matrix (GLRLM) [Conners and Harlow, 1980] in directions θ equal to 0°, 45°, 90° and 135°: short run emphasis, long run emphasis, gray level distribution, run length distribution, and run percentage.

Each feature was calculated on six different areas: four areas centered on the selected pixel, with sizes 7x15, 15x7, 7x3, and 3x7 pixels, and two non-centered areas with sizes 7x3 pixels. In this way we obtained a total of 211 features for all analyzed pixels.

For the feature selection phase the QuickReduct Algorithm (QRA) was chosen, based on the Rough Set Theory (RST).

RST, introduced by Pawlak [Pawlak, 1982], is a powerful tool to model imperfect and incomplete knowledge, which does not require any a-priori information or model assumptions about data.

Given a decision system with discretized attribute values, it is possible to find the minimal subset R (reduct) of the original features, using RST, which is the most informative. The criterion used in order to measure the relevance of the chosen features is the dependency degree $\gamma_C(D)$. It evaluates the dependency of the decision attribute D from the set of the conditional features C and is comprised between 0, if there isn't any dependency, and 1, if all values from D are uniquely determined by values of attributes C.

QRA, introduced in [Shen and Chouchoulas, 2000], is a basic tool allowing to resolve reduct search problems without generating all the possible subsets. It is based on the dependency degree measured between a decision attribute D and a subset of conditional features R analyzed in order to be a reduct. The algorithm starts from an empty subset of features and adds to it those attributes producing a larger increase in the dependency degree, until the maximum dependence value is reached. This means that the final subset R returns a dependency degree equal to the one obtained considering the whole set of the original variables C.

The dataset used for feature selection results in a value $\gamma_C(D)$ equal to 1, which is consistent, and the QRA extracted a subset of 12 parameters.

2.2. Pixels Classification and IMT Estimation

The extracted subset of features was used to classify each pixel in the region of interest by means of a classifier based on three similar ANNs.

A feed-forward structure was chosen for each ANN. The input layer consisted of a number n of neurons equal to the number of extracted features. The structure contained n-1 hidden layers and

terminated with one output neuron only. The number of neurons was progressively reduced of one element through every hidden layer As for the neuron activation functions, we used a logarithmic sigmoid function for the hidden layers and a linear function for the output layer. Back-propagation was chosen as the learning algorithm and the mean squared error was used as performance function. The initial values of interconnection weights were set randomly. Three new datasets were constructed to train the ANNs. As for the dataset used for feature selection every training set was constructed with 600 pixels per class randomly chosen from 60 images randomly selected. Every ANN was trained with a different dataset.

We decided to divide the ultrasound images in small contiguous squares made of 4 pixels. Each area was considered as a single point with an intensity that is the mean of the intensities of the 4 pixels inside it.

A voting system was implemented to classify the pixels. First, the features associated with an area were given as input to each ANN. The results constituted the input of a voting system based on a set of rules. The result of the classifier was the class with at least two votes while if each ANN output was different the area results not classified.

Moreover, two different strategies were used in order to classify the pixels inside the areas. In the first case the output of the voting is directly assigned to all the four pixels inside the considered square (Fig.1A). In the second approach, each pixel was classified to the more represented class among those assigned to the four squares crossing in it (Fig.1B).

An example of the classification result obtained with the first procedure is shown in Fig. 2. The classification obtained with the second procedure was similar.

When all pixels were classified, the LI and MA interfaces were identified as the sequence of the points staying between lumen and intima and between media and adventitia respectively. Firstly the transition zone was detected when at least 5 of 7 consecutive pixels in a column belong to the intima-media complex. Then, the LI and MA profiles were traced following in the middle of these areas. The raw profiles were further elaborated detecting peaks and substituting them with the mean value of the two points around the peak. In this way it was possible to smooth the lines and obtain profiles that follow the anatomic carotid configuration most accurately. The IMT was simply evaluated as the distance between the two profiles. The first testing phase was performed on a set of 50 images randomly selected within the available set.

Two examples of the two interfaces automatically detected with the first classification approach compared with the manual ones are shown in Fig. 3 and Fig. 4 for two images with high and low signal-to-noise ratio respectively.
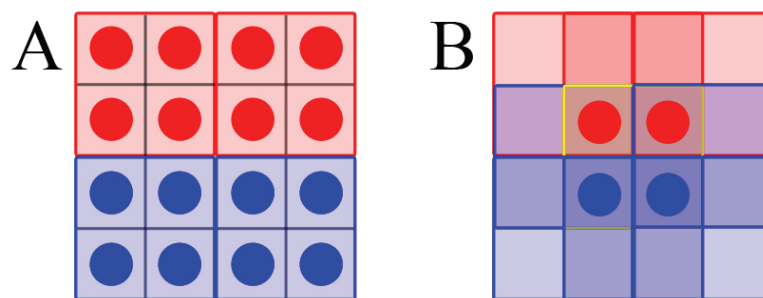

Figure 1. *A) 1st classification procedure: the class assigned to the area is automatically assigned to all pixels inside it. B) 2nd classification method: each pixel is classified using a voting system implemented among the classes assigned to the four squares crossing in it.*
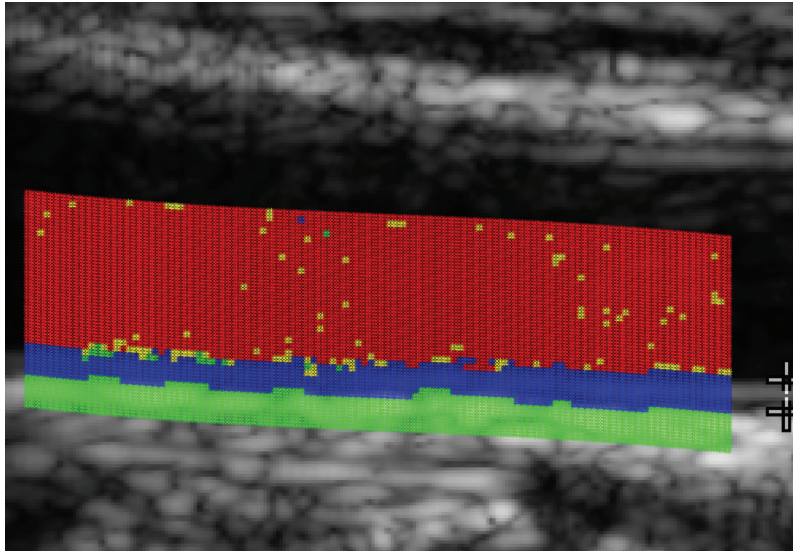
Figure 2. *Example of pixel classification obtained with the first classification approach. The red points identify the lumen pixels, the blue points mark the intima-media complex pixels, the green points represent the adventitia pixels and the yellow points are not classified pixels.*
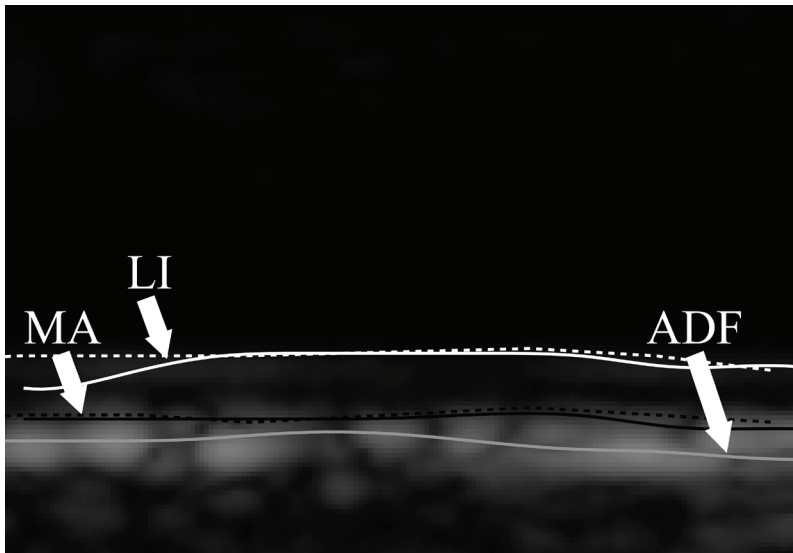

Figure 3. *Example of LI (white lines) and MA (black lines) interfaces automatically traced (solid lines) and manually traced (dashed lines) on a image with high signal-to-noise ratio. The grey line represents the far adventitia layer (ADF).*

Figure 4. *Example of LI (white lines) and MA (black lines) interfaces automatically traced (solid lines) and manually traced (dashed lines) on a image with low signal-to-noise ratio. The grey line represents the far adventitia layer (ADF).*
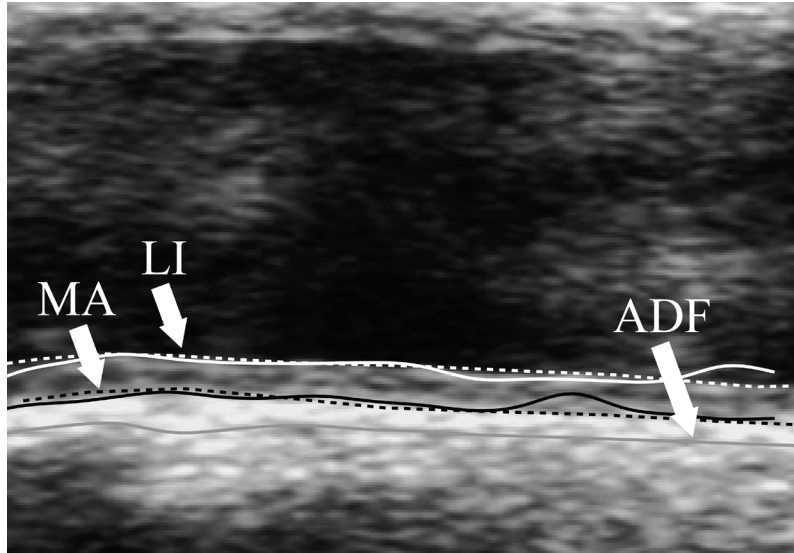
3. Results

The extracted LI and MA profiles were compared with those manually-traced by two human experts. The differences between the three sets of interfaces are shown in Table 1 and Table 2 respectively for the first and the second classification approach, in terms of mean value and standard deviation. Table 1 and Table 2 show that the average LI segmentation error was about 0.2 mm, which is slightly higher than the MA segmentation error (about 0.18 mm). These values were little higher than the inter-reader profile distance, which was about 0.14 mm. In Table 3 and Table 4 are reported the results concerning the IMT evaluated on the automatic profiles respectively for the first and the second classification approach, compared with the manual ones, in terms of mean value and standard deviation.

Table 1. *Mean value and standard deviation relative to the differences between automatic LI and MA interfaces extracted with the first classification approach and two set of human-traced profiles.*

	1st human operator	2nd human operator
Automatic profiles	LI=(0.20±0.14) mm MA=(0.17±0.11) mm	LI=(0.19±0.13) mm MA=(0.18±0.14) mm
1st human operator	-	LI=(0.13±0.06) mm MA=(0.14±0.08) mm

Table 2. *Mean value and standard deviation relative to the differences between automatic LI and MA interfaces extracted with the second classification approach and two set of human-traced profiles.*

	1st human operator	2nd human operator
Automatic profiles	LI=(0.20±0.14) mm MA=(0.15±0.11) mm	LI=(0.21±0.15) mm MA=(0.17±0.13) mm
1st human operator	-	LI=(0.13±0.06) mm MA=(0.14±0.08) mm

Table 3. *Mean value and standard deviation relative to the differences between automatic IMT extracted with the first classification approach and two set of human-traced profiles.*

	1st human operator	2nd human operator
Automatic profiles	(-0,031±0.282) mm	(0.011±0.235) mm
1st *human operator*	-	(0.042±0.247) mm

Table 4. *Mean value and standard deviation relative to the differences between automatic IMT extracted with the second classification approach and two set of human-traced profiles*

	1st human operator	2nd human operator
Automatic profiles	(-0,064±0.286) mm	(-0.021±0.256) mm
1st *human operator*	-	(0.042±0.247) mm

The IMT measurement bias of the automated procedure with the first classification approach results smaller than the one obtained with the second approach. In the first case, in fact, it is of -0.031 mm and 0.011 mm with respect to the first and second human observers, respectively. The inter-readers IMT difference was 0.042±0.247 mm. Thus, the performance of the automated algorithm can be considered as satisfactory for what concern the IMT average measurement error. Moreover, the automatic profiles tends to underestimate the IMT values in all cases, except for the second procedure compared with the 2nd human operator.

Additionally, a Student's t-test was performed taking as first population the distances between automatic IMT and the two manual IMT alternatively and as second population the distances between the two manually-traced IMT, it emerges that the populations are not statistically different with a confidence level of 95%. This means that there are no statistic differences between our IMT results obtained with both classification procedures and the IMT obtained with a manually-traced profiles.

References

Amadasun M, R. King. Textural features corresponding to textural properties. *IEEE Transactions on Systems, Man and Cybernetics*, 19(5):1264-1273, 1989.

Conners RW, Harlow CA. A Theoretical comparison of texture algorithms. *IEEE Transactions on In Pattern Analysis and Machine Intelligence*, 2(3):204-222, 1980.

Pawlak Z. Rough sets. *International Journal of Parallel Programming*, 11(5):341-356, 1982.

Rosati S, Molinari F, Balestra G. Feature selection applied to ultrasound carotid images segmentation. In proceeding of the 33rd Annual International Conference of the IEEE Engineering in Medicine and Biology Society, 2011,5161-5164.

Shen Q, Chouchoulas A. Modular approach to generating fuzzy rules with reduced attributes for the monitoring of complex systems. *Engineering Applications of Artificial Intelligence*, 13(3):263-278, 2000.

Tan JH, Ng EYK, Rajendra Acharya U,Chee C. Study of normal ocular thermogram using textural parameters. *Infrared Physics and Technology*, 53(2):120-126, 2010.

Touboul PJ, Hennerici MG, Meairs S, Adams H, Amarenco P, Desvarieux M, Ebrahim S, Fatar M, Hernandez Hernandez R, Kownator S, Prati P, Rundek T, Taylor A, Bornstein N, Csiba L, Vicaut E, Woo KS, Zannad F. Mannheim intima-media thickness consensus. *Cerebrovascular Diseases*, 18(4): 346-349, 2004.